Astron. Astrophys. 85, 20–25 (1980)

ASTRONOMY AND ASTROPHYSICS

Non-radial Oscillations of a 1 $M_\odot$ Star with an Initial Discontinuity in Chemical Composition

A. Boury, R. Scuflaire, A. Noels, and M. Gabriel

Institut d'Astrophysique de l'Université de Liège, B-4200 Cointe-Ougrée, Belgique

Received May 2, 1979

Summary. The vibrational stability towards non-radial oscillations of a $1 M_\odot$ star with a low or zero initial hydrogen abundance in the inner 3% of the mass, is studied. The star becomes unstable at an age of $5\,10^7$ yr. Stability is restored after one and a half billion years. The star exhibits particular modes associated with the discontinuity in density, which are strongly damped.

The comparison between the predicted period spectrum of the model corresponding to the present sun and the observations is discussed.

Key words: Sun – non-radial oscillations – vibrational stability – stellar pulsation – discontinuity modes

I. Introduction

In attempting to explain the low solar neutrino flux detected by the Brookhaven experiment (Davis 1971, 1978) various non standard models of the structure and the evolution of the Sun were constructed by different authors departing, in one respect or the other, from the usual assumptions of the theory of solar evolution (for a review of these non standard models, see Rood (1978) and Bahcall (1979). Among them (none of which is satisfactory), we find the models built by Faulkner et al. (1975) in which the initial hydrogen content inside a small central region of the Sun is very much smaller than that in the outer layers. Some of their evolutionary models produce low neutrino fluxes, but the photon luminosity reaches the present solar value after a time span much shorter than the age of the Sun. Other sequences yield the right luminosity at present age but provide neutrino fluxes higher than the standard model prediction which is about 5 SNU (Bahcall, 1977). However the failure is not much worse than the standard model's. Moreover the Sun, in its standard evolution, goes through a phase of vibrational instability towards non-radial oscillations (Christensen-Dalsgaard et al., 1974; Boury et al., 1975; Shibahashi et al., 1975). Also the possible observation of the oscillation spectrum of the Sun (Brown et al., 1976, 1978) raises hopes to permit discrimination between various solar models, through solar "seismology" (Scuflaire et al., 1975; Christensen-Dalsgaard and Gough, 1976; Hill and Caudell, 1979). It is thus interesting to study the non-radial oscillations of models of the type constructed by Faulkner et al., all the more because these models will exhibit oscillatory modes connected with the discontinuity in chemical composition. In Sect. II, the principal properties of the models investigated are described. In Sect. III and IV, the non-radial oscillations and the stability of the models are discussed.

Send offprint requests to: A. Boury

II. Models

An evolutionary sequence of a $1 M_\odot$ star of initial hydrogen abundance $X = X_c = 0.1$ in the inner three per cent of the mass and $X = X_s$ in the rest of the star, and of heavy element abundance $Z = 0.02$, was computed by the Henyey method. The opacities were obtained by interpolation in Cox and Stewart's tables (1970). The nuclear reaction rates were taken from Fowler et al. (1975). The ratio l/H_p of the mixing length to the pressure scale height was chosen equal to 1.5. X_s was adjusted to fit the luminosity at evolutionary age $4.7\,10^9$ yr to the present solar luminosity. We find $X_s = 0.7813$. The very slight difference between our X_s and the value 0.790 given by Faulkner et al. (1975) arises from differences in physical input and in the numerical codes. In order to reach the present value of the solar radius within less than one percent, l/H_p was changed to 2.15 in the last models of the evolutionary sequence.

Another evolutionary sequence with $X_c = 0$ and $X_s = 0.794$ was also constructed. The qualitative behaviour of those models with respect to non-radial oscillations turns out to be the same as that of the $X_c = 0.1$ models so no precise adjustement of X_s was made to fit exactly the present solar luminosity and radius.

The properties of the models tested for vibrational stability are listed in Table 1, where x_D, X_{Di} and X_{Do} stand respectively for the fractional distance of the discontinuity in chemical composition to the centre, and the hydrogen abundance on the inner side and on the outer side of the discontinuity. Other symbols have their usual meaning. Models 1, 2, 3 (for $X_c = 0.1$), 7 and 8 (for $X_c = 0$) correspond to the approach to the main sequence. Model 6 corresponds to the present Sun.

III. Non-radial Adiabatic Oscillations

The basic theory of non-radial oscillations can be found in Ledoux and Walraven (1958). We integrated numerically the fourth-order differential system corresponding to the adiabatic problem, taking into account the perturbation of the gravitational potential. The form of the equations and the method of calculation are the same as given in Boury et al. (1975).

Table 1. Properties of the models

Model Number	ℓ/H_p	Age (years)	x_D	X_{Di}	X_{Do}	T_c	ρ_c	L	$\rho_c/\bar{\rho}$
			a) Sequence $X_c=0.1$, $X_s=0.7813$						
1	1.5	4.44(7)	0.06150	0.09987	0.7796	1.392(7)	290.8	2.637(33)	168.3
2	1.5	4.98(7)	0.06508	0.0998 3	0.7791	1.374(7)	295.9	2.612(33)	170.4
3	1.5	5.75(7)	0.06514	0.09978	0.7785	1.358(7)	302.3	2.622(33)	175.4
4	1.5	8.68(8)	0.05720	0.09640	0.7182	1.343(7)	346.3	2.840(33)	220.3
5	1.5	4.70(9)	0.04652	0.07604	0.4190	1.509(7)	471.9	3.750(33)	419.1
6	2.15	4.70(9)	0.04977	0.07582	0.4168	1.513(7)	472.5	3.809(33)	342.1
			b) Sequence $X_c=0$, $X_s=0.794$						
7	1.5	4.83(7)	0.05736	-	0.7919	1.275(7)	507.4	2.546(33)	302.2
8	1.5	5.63(7)	0.06268	-	0.7911	1.275(7)	506.2	2.526(33)	300.3
9	1.5	9.03(8)	0.05152	-	0.7234	1.282(7)	543.3	2.703(33)	351.6
10	1.5	2.50(9)	0.04809	-	0.5951	1.334(7)	589.2	2.994(33)	429.0

Numbers in parentheses indicate the power of 10 which multiplies the preceding numbers.

Table 2. Periods of adiabatic oscillation and vibrational stability results: g-modes of $l=1$ (see text)

Mode	Model	ω^2	P(s)	E_N	E_F	E_{ε_2}	σ^{-1} years[a]
		a) Sequence $X_c=0.1$ $X_s=0.7813$					
g_1	1	7.8780	3.222(3)	6.621(33)	2.005(37)	6.702(36)	3.617(5)
	2	7.8665	3.217(3)	7.055(33)	1.845(37)	6.676(36)	1.728(5)
	3	7.8640	3.230(3)	7.551(33)	1.839(37)	6.132(36)	1.655(5)
	4	7.9046	3.360(3)	1.425(34)	2.267(37)	7.793(36)	1.627(5)
	5	12.696	3.144(3)	5.622(35)	4.512(36)	9.943(35)	9.657(5)
	6	10.425	3.133(3)	5.143(35)	3.720(36)	7.724(35)	1.031(6)
g_2	1	3.2561	5.012(3)	4.805(35)	1.260(36)	1.414(31)	1.080(6)
	2	3.5710	4.774(3)	4.082(35)	1.222(36)	1.278(31)	1.139(6)
	3	3.9404	4.562(3)	3.436(35)	1.204(36)	1.412(31)	1.185(6)
	4	5.8776	3.912(3)	1.818(35)	1.246(36)	5.114(32)	1.289(6)
	5	10.754	3.416(3)	5.943(35)	6.990(36)	2.263(36)	4.350(5)
	6	8.9907	3.374(3)	4.383(35)	8.810(36)	2.953(36)	3.979(5)
g_3	1	2.1934	6.107(3)	2.070(35)	2.123(35)	1.497(33)	1.129(9)
	2	2.2158	6.061(3)	2.243(35)	2.205(35)	4.203(33)	-6.698(7)
	3	2.2795	5.998(3)	2.466(35)	2.311(35)	3.963(33)	-3.576(7)
	4	3.3686	5.167(3)	4.163(35)	3.769(35)	8.044(33)	-1.719(7)
	5	7.9828	3.965(3)	4.918(34)	3.789(37)	1.202(37)	6.913(4)
	6	7.5896	3.672(3)	1.267(35)	1.708(37)	6.405(36)	1.726(5)
g_4	1	1.3049	7.917(3)	2.148(35)	2.775(35)	1.497(33)	5.712(6)
	2	1.3302	7.823(3)	2.022(35)	2.912(35)	1.523(33)	4.067(6)
	3	1.3971	7.662(3)	1.563(35)	8.474(35)	5.851(32)	5.277(5)
	4	2.0993	6.545(3)	7.504(34)	1.308(36)	1.104(32)	4.267(5)
	5	5.0533	4.984(3)	3.404(35)	1.077(36)	9.896(34)	1.791(6)
	6	4.1532	4.964(3)	3.044(35)	7.788(35)	3.196(34)	2.274(6)
g_5	1	1.1075	8.594(3)	1.913(35)	1.175(36)	1.008(31)	2.912(5)
	2	1.2376	8.110(3)	1.553(35)	1.154(36)	4.795(31)	3.214(6)
	3	1.3607	7.764(3)	1.674(35)	5.898(35)	9.837(32)	8.492(5)
	4	1.9029	6.875(3)	1.419(35)	2.713(35)	3.585(33)	3.791(6)
	5	4.4616	5.304(3)	1.615(35)	2.424(36)	4.345(33)	4.431(5)
	6	3.6414	5.301(3)	1.424(35)	2.147(36)	1.499(33)	4.363(5)

a) A negative sign means instability.

Table 2. (Cont'd)

Mode	Model	ω^2	P(s)	E_N	E_F	E_{ε_2}	σ^{-1} years[a]
		b) Sequence $X_c=0$ $X_s=0.794$					
g_1	7	12.016	2.645(3)	8.246(33)	1.420(33)	1.120(33)	2.179(6)
	8	11.501	2.700(3)	9.665(33)	1.587(36)	6.319(32)	1.876(6)
	9	13.506	2.602(3)	1.229(34)	1.850(36)	4.443(33)	1.840(6)
	10	16.174	2.522(3)	2.259(34)	2.024(36)	7.014(34)	2.009(5)
g_2	7	7.8233	3.280(3)	9.341(33)	1.125(37)	6.111(36)	3.772(5)
	8	7.8062	3.278(3)	1.022(34)	1.739(37)	5.568(36)	1.690(5)
	9	7.8625	3.411(3)	2.077(34)	1.775(37)	6.621(36)	3.131(5)
	10	8.1235	3.559(3)	1.738(35)	2.059(37)	6.793(36)	1.436(5)
g_3	7	4.6159	4.272(3)	2.205(33)	1.600(36)	2.180(31)	7.385(5)
	8	4.3704	4.380(3)	2.927(33)	1.652(36)	3.393(31)	6.805(5)
	9	5.1462	4.216(3)	1.169(34)	2.061(36)	6.063(32)	6.271(5)
	10	6.9676	3.843(3)	5.438(35)	3.287(36)	9.102(35)	9.375(5)
g_4	7	2.4960	5.808(3)	4.135(33)	4.497(35)	3.301(33)	2.040(7)
	8	3.0155	5.273(3)	5.231(35)	4.776(35)	2.856(33)	-1.617(7)
	9	4.3921	4.564(3)	5.694(35)	5.628(35)	1.355(34)	-4.828(7)
	10	6.1229	4.100(3)	1.723(34)	1.897(36)	4.739(33)	4.449(5)
g_5	7	2.3755	5.953(3)	2.503(33)	1.536(36)	2.708(33)	4.021(5)
	8	2.2827	6.063(3)	8.094(32)	1.813(36)	1.128(31)	3.232(5)
	9	2.6827	5.839(3)	8.637(32)	2.203(36)	2.045(31)	3.037(5)
	10	3.3025	5.582(3)	2.358(35)	6.273(35)	9.362(33)	4.030(5)

Two remarks should be made, however: first, the presence of the discontinuity of density accompanying the imposed discontinuity in molecular weight makes the behaviour of the eigenfunctions less predictable and more complicated in the central regions, particularly in the neighbourhood of the discontinuity. For instance, modes with close frequencies can exhibit completely different amplitude distributions. The choice of a grid of points, interpolated from the model under study and suitable for the computation of the eigenfunction is no longer possible at the outset of the calculation and it is necessary to use an algorithm optimizing the grid during the calculation.

Second, it is absolutely necessary to make sure that one has chosen a sufficient number of points in the model, for some eigenvalues and eigenfunctions turn out to be very sensitive to the detailed structure of the model. If the grid of the model is not narrow enough, the results can vary appreciably and depend on the method of interpolation among the data of the model. In that case, we find that the interpolation by splines is less satisfactory than the linear interpolation in well chosen variables such as $\ln(m(r)R^3/r^3M)$, $\ln\varrho$ etc.

The eigenfunctions are normalized in such a way that

$$\int \left|\frac{\delta \mathbf{r}}{R}\right|^2 \frac{dm}{M} = 1 \tag{1}$$

If $\mathbf{e}_r$, $\mathbf{e}_\theta$, $\mathbf{e}_\phi$ are the unit vectors in the directions r, θ, ϕ, and if we let

$$\mathbf{e}_1 = \sqrt{4\pi}\, Y_l^m(\theta,\phi)\mathbf{e}_r,\ e_2 = \frac{\sqrt{4\pi}}{[l(l+1)]^{1/2}} \cdot \left(\frac{\partial Y_l^m}{\partial\theta}\mathbf{e}_\theta + \frac{1}{\sin\theta}\frac{\partial Y_l^m}{\partial\phi}\mathbf{e}_\phi\right)$$

$$\int_{4\pi} |\mathbf{e}_1|^2\, d\Omega = \int_{4\pi} |\mathbf{e}_2|^2\, d\Omega = 1$$

then

$$\delta\mathbf{r} = \delta r\,\mathbf{e}_1(\theta,\phi) + \xi_t \mathbf{e}_2(\theta,\phi)$$

Y_l^m is the spherical function

$$\left[\frac{(2l+1)(l-|m|)!}{4\pi(l+|m|)!}\right]^{1/2} P_l^m(\cos\theta)\exp(\mathrm{i}m\phi),$$

P_l^m being the associated Legendre polynomial.

The classification of the modes in g_n, f and p_n modes following Cowling's nomenclature (1941) was made according to the scheme

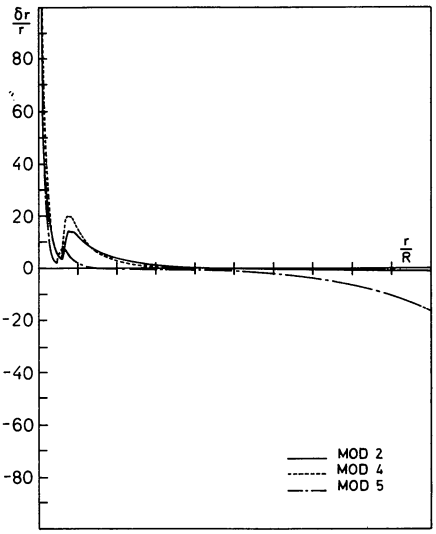

Fig. 1

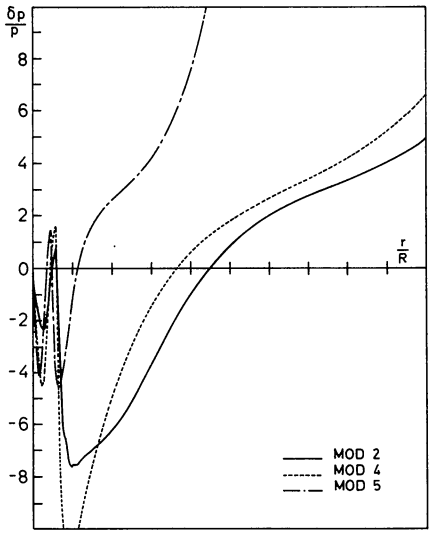

Fig. 2

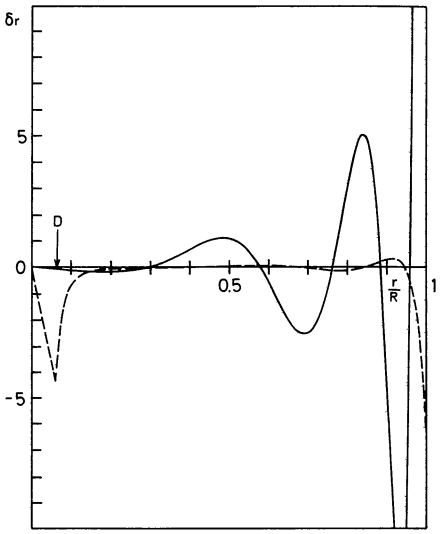

Fig. 3

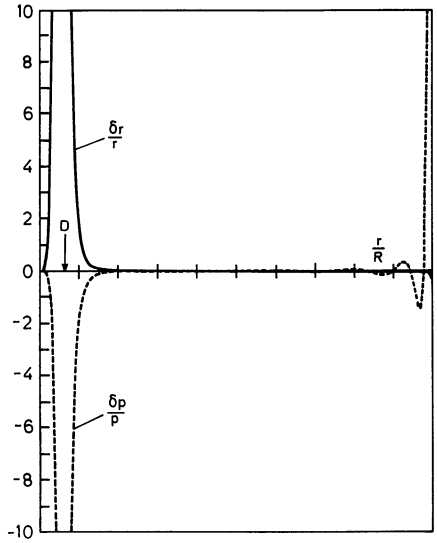

Fig. 4

Fig. 1. Relative amplitude, $\delta r/r$ of radial distance variations versus r/R for the mode $l=1$, g_3 in models 2, 4 and 5

Fig. 2. Relative amplitude, $\delta p/p$ of pressure variations versus r/R for the mode $l=1$, g_3 in models 2, 4 and 5

Fig. 3. Amplitude δr distribution versus $x=r/R$ for the $l=2$, p_4 (dashed line) and p_5 (solid line) modes in model 1. Symbol D marks the position of the discontinuity. The peak at discontinuity is very sharp

Fig. 4. Distribution of amplitude $\delta r/r$ and $\delta p/p$ versus r/R for the $l=6$, p_7 mode. Symbol D marks the position of the discontinuity. The peak at discontinuity is very sharp

developed by Scuflaire (1974) and Osaki (1975). Their classification criterion is proved by Gabriel and Scuflaire (1979) in the case where the perturbation Φ' of the gravitational potential is neglected. In the models studied here, the criterion works even when Φ' is taken into account, except when l the degree of the spherical harmonic is equal to 1. When $l=1$, the criterion gives the correct classification only when the order n of the mode is larger than ~ 10, so the $l=1$ modes with $n<10$ were classified step by step, starting from modes with $n>10$. In columns 3 and 4 of Table 2, we list $\omega^2=R^3\sigma^2/GM$, σ being the angular frequency, and the period P (in seconds) of the modes g_1 through g_5, for $l=1$. Figures 1 and 2 show for the mode g_3, $l=1$ of models 2, 4 and 5 the distribution of the amplitudes of $\delta r/r$, the relative radial displacement and $\delta p/p$, the relative lagrangian pressure oscillation. The difference between the eigenvalues of model 5 and of model 6 comes from the difference in $\varrho_c/\bar{\varrho}$ due to the difference in radius.

The stable discontinuity of density induces, for each l, a particular behaviour of the eigenfunction of one or more modes. At the discontinuity, the amplitude reaches a maximum large compared to the average value equal to 1 (cf. Eq. (1)). As l increases, the phenomenon, still not very conspicuous for $l=1$, becomes more and more pronounced and the peak heightens. Those modes can be called in a rather lax sense, discontinuity modes. Figure 3 shows, for δr *vs* r/R, the behaviour in model 1 of the modes p_4 and p_5 of $l=2$. The p_5 eigenfunction exhibits the usual shape of a p-mode but the p_4 mode is characterized by the larg amplitude near the discontinuity. Figure 4 shows, for the same model, $\delta r/r$ and $\delta p/p$ for the discontinuity mode of $l=6$.
In their behaviour near the discontinuity, the discontinuity modes can be compared to the mode appearing in a stable system of two layers made from different incompressible fluids of densities ϱ_1 and ϱ_2 (Landau and Lifshitz, 1959). The angular frequency of the mode associated with the discontinuity in density is given by

$$\sigma_D^2 \simeq kg\frac{\varrho_1-\varrho_2}{\varrho_1+\varrho_2} \qquad (2)$$

where k is the horizontal wave number and g the gravity. (1) is valid when the width of the two layers is large compared to k^{-1}.

Table 3. Periods of adiabatic oscillations and vibrational stability: discontinuity modes (see text)

a) Model 1

l	Mode	ω^2	P(s)	E_N	E_F	$E_R^r(D)$	E_{ε_2}	σ'^{-1} years
1	p_1	18.605	2.097(3)	6.094(34)	2.289(38)	8.775(34)	7.990(37)	4.901(4)
	p_2	21.825	1.936(3)	5.488(34)	3.998(38)	1.270(35)	1.462(38)	3.008(4)
2	p_4	69.615	1.084(3)	6.168(35)	9.731(37)	1.390(36)	3.886(37)	3.117(5)
3	p_5	113.65	8.483(2)	1.002(36)	1.788(38)	3.554(36)	7.882(37)	2.958(5)
4	p_6	156.63	7.227(2)	1.228(36)	7.506(37)	6.573(36)	2.386(37)	6.099(5)
5	p_7	198.64	6.417(2)	1.389(36)	8.889(37)	1.058(37)	1.830(37)	8.939(5)
6	p_7	240.26	5.835(2)	1.506(36)	1.726(37)	1.556(37)	5.971(35)	4.209(6)
7	p_8	282.13	5.384(2)	1.651(36)	2.006(37)	2.099(37)	1.187(34)	4.097(6)
8	p_9	323.45	5.029(2)	1.732(36)	2.949(37)	2.762(37)	4.970(35)	3.195(6)
9	p_9	364.68	4.736(2)	1.800(36)	3.431(37)	3.513(37)	1.800(31)	3.022(6)
10	p_{10}	405.86	4.489(2)	1.858(36)	4.427(37)	4.352(37)	1.435(35)	2.601(6)

b) Model 8

1	p_2	26.054	1.794(3)	1.013(35)	3.035(38)	2.280(33)	1.179(38)	3.150(4)
2	p_5	119.35	8.382(2)	6.820(35)	6.243(39)	3.190(35)	2.313(39)	7.852(3)
4	p_9	277.24	5.500(2)	1.714(36)	5.922(39)	3.121(36)	1.714(39)	1.781(4)
8	p_{13}	573.71	3.823(2)	2.729(36)	2.801(39)	1.774(37)	7.096(34)	6.342(6)

Table 4. Periods (in minutes) of model 6 ("present Sun") for radial ($l=0$) and non-radial ($l=2, 4, 6, 8$) modes. The identification of the modes is given in parentheses. *D* indicates a discontinuity mode. Last column gives solar periods observed by Brown et al. (1978) in the range 10 min–70 min

l=0	l=2	l=4	l=6	l=8	Observed
	70.7 (g_6)		71.1 (g_{20})	66.6 (g_{20}) 62.2 (g_{19})	
65.9	61.2 (g_5)	67.3 (g_{11}) 64.7 (g_{10}) 62.9 (g_9)	67.4 (g_{16}) 65.2 (g_{15}) 61.3 (g_{14})	61.9 (g_{18})	66.25
	59.4 (g_4) 51.3 (g_3)	56.2 (g_8) 53.0 (g_7)	58.9 (g_{13}) 57.6 (g_{12}) 56.5 (g_{11}) 51.8 (g_{10}) 51.1 (g_9)	59.1 (g_{17}) 55.2 (g_{16}) 55.0 (g_{15}) 52.9 (g_{14}) 51.1 (g_{13})	
41.7	44.8 (g_2)	49.6 (g_6) 43.8 (g_5) 41.5 (g_4)	46.3 (g_8) 42.8 (g_7) 42.0 (g_6)	49.6 (g_{12}) 48.5 (g_{11}) 45.5 (g_{10}) 44.2 (g_9) 42.0 (g_8)	44.66
31.4	39.1 (g_1) 35.5 (f) 32.7 (p_3)	38.4 (g_3) 36.6 (g_2)	37.1 (g_5) 34.9 (g_4) 34.3 (g_3) 31.3 (g_2)	38.0 (g_7) 37.6 (g_6) 33.1 (g_5) 31.4 (g_4) 31.3 (g_3)	39.00 32.1
24.7	25.4 (p_2) 20.8 (p_3)	29.9 (g_1) 28.1 (f) 27.9 (p_1) 22.3 (p_2)	26.5 (g_1) 25.3 (f) 24.7 (p_1) 20.3 (p_2)	28.3 (g_2) 24.7 (g_1) 23.3 (f) 23.2 (p_1)	28.7 24.8 21.0
17.4 15.0 13.3 12.0	17.6 (p_4) 16.3 (p_5)D 15.3 (p_6) 13.5 (p_7) 12.1 (p_8) 11.0 (p_9) 10.1 (p_{10})	18.5 (p_3) 15.9 (p_4) 14.0 (p_5) 12.8 (p_6) 11.4 (p_7)D 11.3 (p_8) 10.3 (p_9) 9.53(p_{10})	17.1 (p_3) 14.8 (p_4) 13.1 (p_5) 11.77(p_6) 10.71(p_7) 9.84(p_8) 9.46(p_9)D	18.8 (p_2) 16.0 (p_3) 13.9 (p_4) 12.4 (p_5) 11.1 (p_6) 10.2 (p_7) 9.40(p_8)	19.5 13.3 12.1 11.4 10.7 9.9

In the stellar case, taking $k=\dfrac{l}{r}$, (2) becomes

$$\omega_D^2 \simeq \frac{l}{r}\frac{R^3}{r^3}\frac{m(r)}{M}\frac{\varrho_{Di}-\varrho_{Do}}{\varrho_{Di}+\varrho_{Do}} \tag{3}$$

where ϱ_{Di} and ϱ_{Do} are the densities on the inner side and on the outer side of the discontinuity. In model 1, $x_D=0.065$, $\varrho_{Di}=181$, $\varrho_{Do}=93$, $\omega_D^2 \simeq 41l$ which can be compared to the values taken from Table 3, where ω^2 and P for the discontinuity modes of $l=1$ through 10 in model 1, are given: Eq. (3) gives a good approximation for the ω^2 of the discontinuity modes as soon as $l \simeq 4$.

The place of the discontinuity modes in the spectrum is also indicated in Table 3. It should be emphasized that, for low-order (non asymptotic) modes, the classification procedure, using Cowling's nomenclature, introduced by Scuflaire (1974) and Osaki (1975) is made with the help of the number of nodes of $\delta r/r$ and $\delta p/p$ and with the order of their appearance from the centre to the surface. The "discontinuity" modes are characterized by a high amplitude at the discontinuity but, otherwise, they obey the classification rule of Scuflaire (1974) and Osaki (1975) and take place in the ordering of *g*, *f* and *p* modes. Let us recall that low-order modes, whether *g* or *p*, can in somewhat condensed models, have the character of an acoustic mode in the outer parts of the star and of a gravity mode in the inner parts.

Besides having the observed solar luminosity and radius any model of the present sun must also yield the observed neutrino flux and predict the correct spectrum of oscillation periods. As shown by Faulkner et al. (1975), the present solar model, such as computed here, yields too high a neutrino flux. Using Bahcall's neutrino capture cross sections, model 6 produces 7.7 SNU. As far as solar seismology is concerned, Table 4 gives the periods predicted from model 6 in the range 10 min $-$70 min for $l=0$ (radial modes), 2, 4, 6 and 8, and comparison can be made with Brown et al. observations (1978) listed in the last column. In the standard sun and in the present solar model resulting from an evolution with intermittent mixing (Scuflaire et al., 1975), a period of about 60 min corresponds to the *f*-mode or to a low order (g_1) mode for $l=2$ and $l=4$. Here it corresponds to higher order *g* modes. The spectrum in the range 30 min $-$60 min is far more compact than the observed spectrum. This compactness arises from the high central condensation of the model, due to the very low initial central abundance of hydrogen. Of course, for each *l*, a few modes only could be excited. We have examined the behaviour of the amplitude of the high order modes, which can be put in two classes: for $l=6$, the modes g_7, g_{10}, g_{12} and g_{16} are trapped under the discontinuity. On the contrary, the remaining modes between g_6 and g_{17} have lower amplitudes in that region and their amplitude at the surface evolves regularly, from one mode to the other, with a sudden maximum for the g_{13} mode. For $l=8$, the modes g_9, g_{12}, g_{16} and g_{19} are trapped. Among the other modes, between g_{10} and g_{20}, the mode g_{14} has a very large amplitude at the surface. There seems to be nothing which obviously favours the excitation of the modes of frequencies close to the observations.

IV. Vibrational Stability

The damping coefficient $\sigma'_{k,l}$ relative to the *k* mode associated with the value *l* of the degree of the spherical function is written in the same form as in Boury et al. (1975)

$$\sigma'_{k,l} = -\frac{1}{2}\left(\frac{E_N - E_F + E_{\varepsilon_2}}{\sigma^2 \int_0^M |\delta\mathbf{r}|^2 dm}\right)_{R,l} \tag{4}$$

with

$$E_N = \int_0^{M_a} \frac{\delta T}{T}\delta\varepsilon\, dm \tag{5}$$

$$E_F = \int_0^{M_a} \frac{\delta T}{T}\delta\left(\frac{1}{\varrho}\nabla\cdot\mathbf{F}\right) dm \tag{6}$$

$$E\varepsilon_2 = \int_0^{M_a} (\Gamma_3 - \tfrac{5}{3})\frac{\delta\varrho}{\varrho}\delta\left(\varepsilon_2 + \frac{1}{\varrho}\bar{\nabla}\cdot\nabla p\right) dm \tag{7}$$

All symbols have the same meaning as in Boury et al. (1975). E_N stands for the contribution of the perturbation of the nuclear energy to the energizing of the pulsation, E_F gives the effect of the

Table 5. Detailed contributions to the vibrational stability coefficient (see text)

Mode		E_R^r	E_C^r	E_R^h	E_C^h	E_5	E_6
Model 2 $\ell=1$	g_1	-3.717(36)	2.260(37)	8.806(34)	-4.931(35)	-2.125(31)	-2.989(34)
	g_2	7.236(35)	5.368(31)	3.792(35)	-1.991(30)	1.653(35)	-4.655(34)
	g_3	7.864(34)	1.817(34)	4.524(34)	-8.495(32)	1.175(35)	-3.824(34)
	g_4	1.749(35)	5.517(33)	4.197(34)	-7.327(31)	7.716(34)	-8.257(33)
	g_5	8.508(35)	1.690(32)	2.346(35)	-1.837(30)	9.732(34)	-2.939(34)
$\ell=6$	p_7	8.182(36)	2.957(36)	7.202(36)	-1.555(33)	-1.041(36)	-3.740(34)
Model 4 $\ell=1$	g_1	-4.251(36)	2.471(37)	9.923(34)	-5.722(35)	4.215(32)	-3.306(34)
	g_2	8.532(35)	1.799(33)	4.027(35)	-5.688(31)	9.529(34)	-2.866(34)
	g_3	1.234(35)	4.196(34)	7.034(34)	-1.755(33)	1.861(35)	-4.321(34)
	g_4	1.011(36)	5.382(32)	2.537(35)	-2.163(31)	6.165(34)	-1.915(34)
	g_5	1.868(35)	1.712(34)	3.179(34)	-6.973(32)	4.297(34)	-3.855(33)
Model 6 $\ell=1$	g_1	8.218(35)	2.251(36)	5.239(35)	-3.844(34)	2.048(35)	-4.618(34)
	g_2	-3.729(35)	8.992(36)	2.545(35)	-1.905(35)	1.841(35)	-5.731(34)
	g_3	-3.325(36)	2.081(37)	1.247(35)	-5.521(35)	6.738(34)	-4.824(34)
	g_4	-5.275(35)	1.265(35)	8.196(34)	-6.023(33)	6.928(34)	-2.044(34)
	g_5	1.648(36)	6.668(33)	4.260(35)	5.154(32)	9.915(34)	-3.155(34)

perturbation of the flux, radiative and convective. The last integral, E_{ε_2} expresses the influence of the mechanical effects of convection; ε_2 represents the rate per unit mass of dissipation of turbulent kinetic energy into heat (Ledoux and Walraven, 1958). The integrals (5), (6) and (7) are carried up to the value M_a of the mass where the adiabatic approximation is no longer valid (Ledoux, 1965).

Columns 5, 6 and 7 of Table 2 give the values of E_N, E_F, E_{ε_2} and of the damping time $1/\sigma'$ for the low order g modes of $l=1$ in the different models studied. A negative sign in front of $1/\sigma'$ means that the mode is vibrationally unstable and that its amplitude grows with the e-folding time $|1/\sigma'|$.

Columns 5, 6, 8 and 9 of Table 3 give the same quantities for "discontinuity modes" in models 1 and 8.

E_F can be written

$$E_F = E_R^r + E_C^r + E_R^h + E_C^h + E_5 + E_6$$

$$E_R^r = \int_0^{M_a} \frac{\delta T}{T} \frac{d\delta L_R^r}{dm} dm \tag{8}$$

$$E_C^r = \int_0^{M_a} \frac{\delta T}{T} \frac{d\delta L_C^r}{dm} dm \tag{9}$$

$$E_R^h = -\int_0^{M_a} \frac{\delta T}{T} \frac{l(l+1)}{\varrho r^2} \delta F_R^h \, dm \tag{10}$$

$$E_C^h = -\int_0^{M_a} \frac{\delta T}{T} \frac{l(l+1)}{\varrho r^2} \delta F_C^h dm \tag{11}$$

$$E_5 = -\int_0^{M_a} \frac{\delta T}{T} \frac{l(l+1)}{\sigma^2 r^2} \chi \frac{d(L_R + L_C)}{dm} dm \tag{12}$$

$$E_6 = \int_0^{M_a} \frac{\delta T}{T} \frac{l(l+1)}{\sigma^2 r^2} \chi \frac{F_R^r + F_C^r}{\varrho r} dm \tag{13}$$

where subscripts R and C mean respectively radiative and convective, while superscripts r and h refer to the radial and horizontal components of the perturbation of the vector fluxes $\mathbf{F}_R$ and $\mathbf{F}_C$. Table 5 gives, for some models, the contributions (8) through (13) to E_F.

A detailed discussion of integrals (5)–(13) is developed in Boury et al. (1975). E_N is destabilizing and E_F is stabilizing in all models, alhough some of the contributions (8)–(13) can be negative. The influence of each depends on the distribution, in the model, of the amplitudes of the mode considered. For instance, in model 2, the $l=1$, g_1 mode has a large amplitude for $r/R>0.2$ so that near the base of the convective envelope, the rapid fall of the radiative luminosity causes δL_R^r to decrease outwards, while δT is positive. This overcomes the stabilizing influence of the inner layers and E_R^r is negative and destabilizing. The large amplitudes in the convective zone, however, give a large value to E_C^r, strongly stabilizing the oscillation. The g_2 mode, on the contrary, has very small amplitudes in the region $r/R>0.2$. The layer where the radiative luminosity decreases has a negligible effect on E_R^r, which reflects the stabilization of the deeper layers. E_C^r is also very small, as well as E_{ε_2}.

In the sequence corresponding to $X_c=0.1$, the $l=1$, g_3 mode becomes unstable, through E_N, at model 2, close to the minimum in the ratio $\varrho_c/\bar{\varrho}$, corresponding to the slight expansion of the central regions, accompanying the onset of nuclear reactions, at the approach to the main sequence.

The instability lasts until $\varrho_c/\bar{\varrho}$ has grown enough again to make the amplitudes in the envelope large enough to damp the pulsation, through E_c^r. Stability is restored at about age $1.6\,10^9$ yr when $\varrho_c/\bar{\varrho} \simeq 245$. Thus, model 6, of present solar age, is stable. The differences between models 5 and 6 arise from the difference in mixing length and radius, which gives a large difference in $\varrho_c/\bar{\varrho}$ influencing the eigenvalues and the eigenfunctions. Since $\varrho_c/\bar{\varrho}$ decreases with increasing l/H_p, the instability duration will be larger in the evolution with $l/H_p=2.15$.

In the sequence $X_c=0$, instability takes place in the $l=1$, g_4 mode. The qualitative aspects remain the same: appearance of the instability near the minimum in $\varrho_c/\bar{\varrho}$ and restabilization when $\varrho_c/\bar{\varrho}$ has reincreased sufficiently. The duration of the phase of instability is large compared to the e-folding time of amplitude growth (Table 2). The shift of the instability to the g_4 mode comes from the difference in $\varrho_c/\bar{\varrho}$ between the two sequences of evolution: not only as far as frequencies are concerned, but also in the general shape of the eigenfunctions, mode g_n of sequence $X_c=0$ resembles mode g_{n-1} of sequence $X_c=0.1$, the additional node appearing in the more dense central region.

The standard solar evolution going through models appreciably less condensed than the present ones, meets a phase of instability towards the $l=1$ g_2 and g_3 modes. The instability lasts

somewhat longer, about 2.5 10^9 yr, because of the smaller values of $\varrho_c/\bar{\varrho}$.

Consider the boundary condition at the surface [Boury et al. (1975), Eq. (13)] which writes, neglecting Φ'.

$$\left(\frac{\delta P}{P}\right)_s \simeq \left[4+\omega^2-\frac{l(l+1)}{\omega^2}\right]\frac{\delta r_s}{R} \tag{14}$$

For $l=1$, $(\delta P/P)_s$ and $(\delta T/T)_s$ will be small around $\omega^2=0.45$. The influence of the outer layers will thus be small for modes around that value of ω^2, which could favour the destabilizing nuclear term E_N. However, in model 2, for instance, $\omega^2=0.55$ and 0.40 correspond to the modes g_8 and g_9 which already present several nodes in $\delta T/T$ in the region $(0.03 \leqq q \leqq 0.15)$ of important nuclear energy generation, so on the average, $\delta T/T$ is smaller than in the g_2 or g_3 modes.

Moreover, the narrow spatial oscillation of the amplitude of those inner layers brings an important stabilizing contribution through E_R^r. The expression for $\delta L/L$ in integral (8) contains a term (Boury et al., 1975, Eq. (26)) $d(\delta T/T)/d\log T$, giving in (8) contributions which can be written, considering, for this argument, this term alone,

$$\begin{aligned}\int \frac{\delta T}{T}\frac{d\delta L}{dx}dx &\simeq \bar{L}\int \frac{\delta T}{T}\frac{d}{dx}\left(\frac{d}{dx}\left(\frac{\delta T}{T}\right)\Big/\frac{d}{dx}\log T\right)dx \\ &= \bar{L}\int \frac{\delta T}{T}\frac{d^2}{dx^2}\left(\frac{\delta T}{T}\right)\Big/\frac{d}{dx}(\log T)dx \\ &+ \bar{L}\int \frac{\delta T}{T}\frac{d}{dx}\frac{\delta T}{T}\frac{d}{dx}\left(\frac{1}{\dfrac{d}{dx}(\log T)}\right)dx\end{aligned} \tag{15}$$

The first integral will be positive while the second will be small. That stabilizing effect is not altered by the small influence of the outer layers.

Higher order g modes and p modes have large amplitudes in the outer layers and are very stable.

The stability was also checked for g modes of $l=2$ and 4. All models are stable. The amplitudes decrease towards the center as r^l, and E_N tends to be smaller with respect to E_F. In higher-l modes, the horizontal temperature gradients will add to stability.

The modes associated with the discontinuity turn out to be very stable (Table 3). The destabilizing maximum of nuclear energy is again largely overcome by the large perturbation of the temperature gradient. Near the discontinuity, the amplitude of the discontinuity mode can be expressed, in a first approximation, as $\exp(\lambda(x-x_D))$ for $x<x_D$ and as $\exp(\lambda(x_D-x))$ for $x>x_D$. Integral (15), carried on the domains $[0, x_D[$ and $]x_D, \infty]$, yields the destabilizing contribution $\lambda\left(\frac{\delta T}{T}\right)_D L\Big/\left(\frac{d\log T}{dx}\right)$, while the discontinuity brings the contribution

$$E_R^r(D)\equiv\left[\left(\frac{\delta T}{T}\right)_D L\left(\frac{\delta L}{L}\right)_{x_D^+}-\left(\frac{\delta L}{L}\right)_{x_D^-}\right]=-\frac{2\lambda L(\delta T/T)_D^2}{\dfrac{d\log T}{dx}}$$

where the subscript D refers to a value calculated at the discontinuity. The global effect is thus very stabilizing. Seventh column of Table 3 shows this contribution to integral (8). A steep profile of hydrogen distribution and of density would have the same stabilizing effect as the strict discontinuity on the modes with a large amplitudes at the steep density change.

V. Conclusions

A star of solar mass with an initial low or zero-hydrogen abundance in a small central region and a normal composition in the rest of the mass, will meet the same instability towards one low-order g mode. Instability appears earlier than in the standard solar evolution, at age 5 10^7 yr and holds until age 1.6 10^9 yr, the phase of instability being appreciably shorter than in the standard evolution. However the growth time of the amplitude is never short compared to the Kelvin-Helmholtz time scale but is short relative to the duration of the instability. The modes associated to the discontinuity are all strongly damped. The spectrum of periods of a present solar model coming from the evolution studied here is much more compact than the observed spectrum.

Acknowledgment. All calculations were performed on the IBM 370-158 of the computing centre of Liège University.

References

Bahcall, J.N.: 1977, *Astrophys. J. Letters* **216**, L115
Bahcall, J.N.: 1978, *Rev. Mod. Phys.* **50**, 881
Bahcall, J.N.: 1979, *Space Sci. Rev.* (to be published)
Boury, A., Gabriel, M., Noels, A., Scuflaire, R., Ledoux, P.: 1975, *Astron. Astrophys.* **41**, 279
Brown, T.M., Stebbins, R.T., Hill, H.A.: 1976, in Proceedings of the Solar and Stellar Pulsation Conference, Los Alamos, N. Mex., ed. A. N. Cox and R. G. Deupree, Los Alamos Report No. LA-6544-C, p. 1
Brown, T.M., Stebbins, R.T., Hill, H.A.: 1978, *Astrophys. J.* **223**, 324
Christensen-Dalsgaard, J., Gough, D.O.: 1976, *Nature* **259**, 89
Christensen-Dalsgaard, J., Dilke, F.W.W., Gough, D.O.: 1974, *Monthly Notices Roy. Astron. Soc.* **169**, 429
Cox, A.N., Stewart, J.N.: 1970, *Astrophys. J. Suppl.* **19**, 261
Cowling, T.G.: 1941, *Monthly Notices Roy. Astron. Soc.* **101**, 367
Davis, R., Jr.: 1971, in *The Astrophysical Aspects of the Weak Interactions*, Academia dei Lincei, Rome, p. 59
Davis, R., Jr.: 1978, in *Status and Future of Solar Neutrino Research*, ed. G. Friedlander, Brookhaven National Laboratory, Upton, N.Y., Vol. 1, p. 1
Faulkner, D.J., Da Costa, G.S., Prentice, A.J.R.: 1975, *Monthly Notices Roy. Astron. Soc.* **170**, 589
Fowler, W.A., Caughlan, G.R., Zimmerman, B.A.: 1975, *Ann. Rev. Astron. Astrophys.* **13**, 69
Gabriel, M., Scuflaire, R.: 1979, *Acta Astronomica*, to be published in Vol. **29**
Hill, H.A., Caudell, T.P.: 1979, *Monthly Notices Roy. Astron. Soc.* **186**, 327
Landau, L., Lifschitz, E.: 1959, Fluid Mechanics, Pergamon, New York
Ledoux, P.: 1965, in *Stars and Stellar Systems*, ed. L. H. Aller and D. Mc Laughlin, Univ. of Chicago Press, p. 543
Ledoux, P., Walraven, Th.: 1958, *Hdb. der Phys.* **51**, 353
Osaki, Y.: 1975, *Publ. Astron. Soc. Japan* **27**, 237
Rood, R.T.: 1978, in *Status and Future of Solar Neutrino Research*, ed. G. Friedlander, Brookhaven National Laboratory, Upton, N.Y., Vol. 1, p. 175
Scuflaire, R.: 1974, *Astron. Astrophys.* **36**, 107
Scuflaire, R., Gabriel, M., Noels, A., Boury, A.: 1976, *Astron. Astrophys.* **45**, 15
Shibahashi, H., Osaki, Y., Unno, W.: 1975, *Publ. Astron. Soc. Japan* **27**, 401